2022 4th International Conference on Sustainable Technologies for Industry 4.0 (STI), 17-18 December, Dhaka

Segmentation of Hemorrhagic Areas in Human Brain from CT Scan Images

Abu Noman Md Sakib, Nipa Anjum, and Sk. Md. Masudul Ahsan
Department of Computer Science and Engineering
Khulna University of Engineering & Technology, Khulna-9203, Bangladesh
Email: abunomanmd.sakib@gmail.com, nipaanjum1998@gmail.com, smahsan@cse.kuet.ac.bd

***Abstract*—Brain hemorrhage is potentially a fatal condition that results from internal bleeding in the human brain. In this study, Computed Tomography (CT) scan images have been used for segmentation tasks to pinpoint the area of hemorrhage. Unique data augmentation techniques using non-linear transformations like, Twirl and Spherical have been used along with traditional data augmentation techniques to increase variation in the dataset. The hemorrhagic portion of the brain in images that are easy to distinguish have been annotated to perform the segmentation task. The segmentation task was applied using U-Net and U-Net++ architecture. U-Net architecture has shown 84.33% Intersection over Union (IoU) and 91.34% dice coefficient score whereas U-Net++ has achieved 17.06% IoU and 28.27% dice coefficient score after applying some non-linear transformations on the dataset.**

***Index Terms*—Segmentation, Brain Hemorrhage, Deep Learning, CT Scan Image, Non-linear Transformation.**

I. Introduction

An accident, brain tumor, stroke or high blood pressure can cause bleeding inside the human brain which leads to damage in brain cells, and the damage results in brain hemorrhage [1]. Among 144 patients, it was proved that 95 patients' cause of hemorrhage is aneurysm, angioma, arteritis, neoplasm, or a blood dyscrasia [2]. According to reports, up to 97% of people with a diagnosis of subarachnoid hemorrhage have severe headaches as symptoms [3]. As the time passes, the damage inside human brain increases if proper steps are not taken.

For brain hemorrhage treatment, doctors first diagnose it by observing different symptoms and then locate the area of hemorrhage by visualizing CT scans, MRI images, angiogram, computed tomography angiography, cerebrospinal fluid exam, or a lumbar puncture. As the treatment primarily depends on the size and location of the bleeding area, localization of hemorrhage within a short time can be helpful as well as an effective approach. If any automated system detects the hemorrhage and then classifies it, the initial process of treating patients can be faster.

Over the years, there has been a lot of work using many methods to efficiently perform the segmentation task of Brain Hemorrhage. Some of those methods used various image processing techniques while some used machine learning and deep learning models to resolve the task of Brain Hemorrhage segmentation. Fuzzy C-Means, or K-Means clustering, Otsu's method, or comparison with the expected histogram are some of the ways. Upon determining an acceptable threshold, using region growth, active contouring, and voxel neighborhood analysis improved result can be achieved. Many convolutional neural network architectures for hemorrhage classification, as well as segmentation, have been developed as a result of the rise of deep learning [4].

This research work contributes to an annotated dataset where two types of non-linear transformation that are twirl and spherical transformation have been used to add variation to the original dataset. Also two state-of-the-art models, U-Net [5] and U-Net++ [6] have been used and compared the performance by measuring the Intersection over Union (IoU) and dice co-efficient. Also using technologies like this reduce the time to detect the problem and increase sustainability in medical treatments.

II. Related Works

Vincy and Satish [7] used the Watershed algorithm to perform the segmentation task using 35 human brain CT scan images. The Sobel operator was used to detect the edges. Some morphological operations such as opening and closing were done and then segmented using the watershed algorithm. Using the segmented images, the features were extracted using GLCM (Grey Level Co-occurrence Matrix) classifier. The extracted features were fed into an Artificial Neural Network (ANN). The resulting detection was measured by error value which was 0.47838 for ICH. The dataset used in this research was very small. The resulting metrics were not unveiling the proper results of the research.

Ali et al. [8] proposed the segmentation of hemorrhagic images by combining multiple image processing techniques. The images were converted into grayscale images from RGB. To remove the noise, a median filter was used and thresholding was applied with a value of 153. The statistical features were calculated using the first order histogram. The results were evaluated by mean, energy, entropy, variance, standard deviation, skewness, and kurtosis. The value comparison of these metrics distinguishes the image between normal and abnormal.

Arif and Wang [9] proposed Midline detection, a segmentation based approach where fuzzy c-mean was utilized to extract features using GLCM and they also used adaptive neuro-fuzzy inference. The proposed method was performed on a dataset of 230 images with 3 classes calcification,

978-1-6654-9045-0/22/$31.00

hemorrhage and both. The method achieved 98.40% accuracy on a small dataset. But this method has not been tested on a large dataset yet. Majumdar et al. [10] used Deep Learning to detect Intracranial Hemorrhage. The dataset had 134 images of five different types. They had done some modification on the U-Net model architecture. Two forms of data augmentation techniques were applied to improve the performance of the model. 81% sensitivity rate and 98% specificity rate were confirmed for the model.

The majority of the studies looked at fundamental image processing techniques or feature extraction, as well as machine learning and direct deep learning techniques to solve classification or segmentation related problems. In image processing-based techniques, different noise removal and smoothing operations, morphological operations such as opening and closing using erosion and dilation and many more methods had been utilized. In machine learning based approach, many models have been reviewed with different classifiers and different model structures. Deep learning-based approaches use Convolutional Neural Network (CNN) with variable hidden layers, neuron counts, different optimizers, fine tuning and so on. Some methods have used Hybrid models, CNN models and pre-trained models to perform the detection and segmentation of various datasets.

III. Methodology

Segmentation is one of the most significant procedures in computer vision where the object of the same category in an image is grouped together. Pixel-level classification is done in segmentation which entails dividing pictures into several segments. In the beginning, image segmentation was done using thresholding [11], K-means clustering [12], histogram-based bundling [13], region growing [14] and some other methods. In deep learning, there are some image segmentation models that performs outstandingly on publicly available benchmark datasets. For brain hemorrhage segmentation, hemorrhagic images were used to create the mask of the portion where the hemorrhage occurred. These images have been used to feed into the deep learning model to learn to automatically segment when a new example comes. Fig. 1 shows the complete work flow of the segmentation process.

A. Dataset Development

In the preprocessing step, some clearly understandable hemorrhagic images from Head-CT Hemorrhage [15] dataset were chosen to create the mask for those images with the help of a doctor. Among 100 hemorrhagic images, 66 images were selected that can be identified as hemorrhagic images in general. Selected 66 hemorrhagic images have been annotated using an online image annotation tool, VGG Image Annotator (VIA) [16]. Non-linear transformations such as Twirl transformation and Spherical transformation were used to increase the number of images, resulting in a total of 726 images. Table I shows the number of images that have been used in training and evaluating the model.

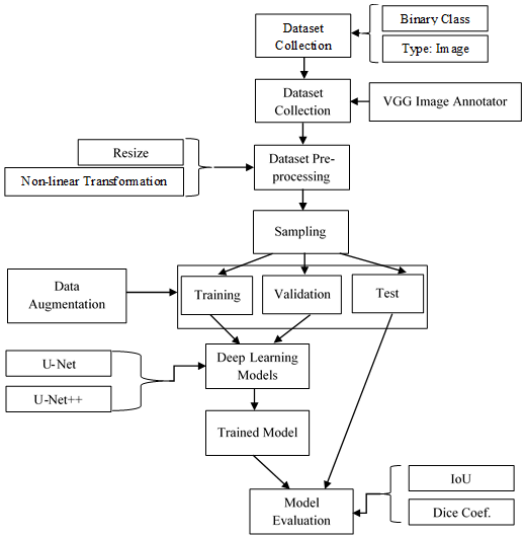

Fig. 1: Flow chart of hemorrhage segmentation process.

TABLE I: Dataset Arrangement

No of images	Train set	Test set	Total
Before non-linear transformation	56	10	66
After non-linear transformation	616	110	726

B. Non-linear Transformation

By using pixel manipulation and geometric transformation, variation can be increased in each hemorrhagic image. Twirl transformation and spherical transformation have been introduced in order to increase variation among selected 66 hemorrhagic images for segmentation. As hemorrhage can occur anywhere and the hemorrhagic area can take any irregular shape, both these transformations have been performed only on the hemorrhagic portions of the image and mask.

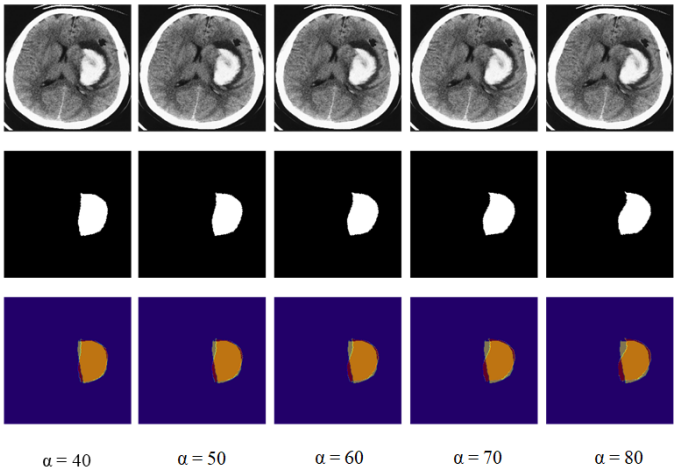

Fig. 2: Twirl transformation on hemorrhagic image and mask.

1) Twirl Transformation: The hemorrhagic portion is rotated by α angle at the center of the hemorrhage which can be denoted as (x_c, y_c). If there are multiple areas of hemorrhage, the centroid is calculated to apply the rotation. It is then increasingly rotated up to a maximum radial (r_{max}) area and the area outside this radial distance has been unchanged. Equation (1-6) has been used to apply the twirl transformation [17].

$$x = \begin{cases} x_c + r \times \cos\beta, & \text{for } r \leq r_{max} \\ x', & \text{for } r > r_{max} \end{cases} \tag{1}$$

$$y = \begin{cases} y_c + r \times \cos\beta, & \text{for } r \leq r_{max} \\ y', & \text{for } r > r_{max} \end{cases} \tag{2}$$

$$d_x = x' - x_c \tag{3}$$

$$d_y = y' - y_c \tag{4}$$

$$r = \sqrt{d_x^2 + d_y^2} \tag{5}$$

$$\beta = \arctan(d_y, d_x) + \alpha \times \left(\frac{r_{max} - r}{r_{max}}\right) \tag{6}$$

2) Spherical Transformation: By applying the spherical transformation, the center of the hemorrhage is zoomed in which is similar to looking through a lens. Equation (3-5) and (7-11) have been used to apply the spherical transformation [17]. The hemorrhagic area is rotated at the center (x_c, y_c) of the hemorrhage and the rotation takes place within the maximum radius (r_{max}).

$$x = x' - \begin{cases} z \times \tan\beta_x, & \text{for } r \leq r_{max} \\ 0, & \text{for } r > r_{max} \end{cases} \tag{7}$$

$$y = y' - \begin{cases} z \times \tan\beta_y, & \text{for } r \leq r_{max} \\ 0, & \text{for } r > r_{max} \end{cases} \tag{8}$$

$$z = \sqrt{d_{max}^2 + d^2} \tag{9}$$

$$\beta_x = (1 - \frac{1}{\rho}) \times \sin^- 1\left(\frac{d_x}{\sqrt{d_x^2 + z^2}}\right) \tag{10}$$

$$\beta_y = (1 - \frac{1}{\rho}) \times \sin^- 1\left(\frac{d_y}{\sqrt{d_y^2 + z^2}}\right) \tag{11}$$

In twirl transformation, the value of rotation angle α has been chosen 40, 50, 60, 70 and 80 degrees. 10-degree increase in angle has been applied on each image that gave a total of 330 transformed images. Similarly, for spherical transformation, the value of reflection index, ρ has been chosen 1.12, 1.14, 1.16, 1.18 and 1.20 that gave 330 transformed images. Also some commonly used augmentation techniques like clockwise rotation range of 0 to 20 degree, height, width shift range and zooming range of 5% and flipping have also been applied.

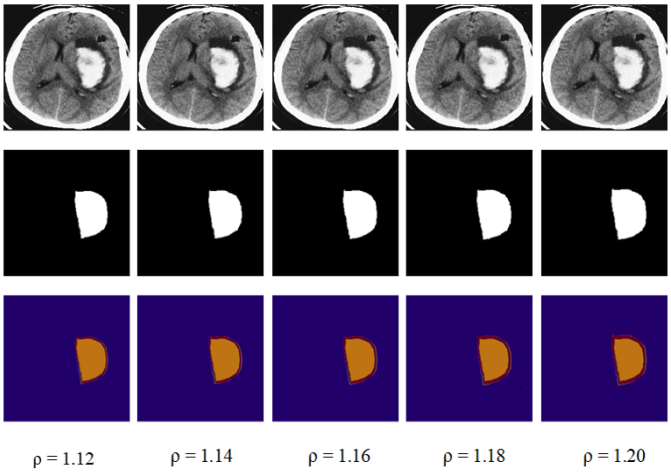

Fig. 3: Spherical transformation on hemorrhagic image and mask.

3) U-Net Architecture: One of the mostly used semantic segmentation architecture is U-Net [5],[18] architecture that has two paths: one that contracts and the other one that expands. In the contracting path, there are two 3×3 convolutions that are applied repeatedly with rectified linear unit as activation and 2×2 max pooling operation with stride 2 for down sampling. The number of feature channel is doubled at each down sampling. In the expanding path, the feature map is up sampled in every step. Two 3×3 convolutions with rectified linear unit as activation function along with the corresponding feature map from the contract path were then concatenated. 1×1 convolution is used in the final layer.

4) U-Net++ Architecture: In U-Net++ [6] architecture, each step is initialized by using a standard unit which consists of two 3×3 convolution layers and two dropout layers with 50% dropout rate. Each individual standard unit operation is followed by a 2×2 max pooling operation with stride 2 for down sampling. The blocks are upsampled and concatenated by using the output of previous concatenations. It creates multiple nested operations and produces four outputs with respect to the four standard units. The usage of deep supervision allows to select which outputs to use. The encoder and decoder sub-networks are connected through a series of nested, dense skip pathways. The redesigned skip paths that connect the encoder and decoder sub-networks, as well as the usage of deep supervision, separate U-Net++ from U-Net.

IV. Result and Discussion

The result of brain hemorrhage can be discussed in two parts for better understanding.

A. Quantitative Results of Segmentation

To evaluate the performance of segmentation model, dice coefficient and Intersection over Union (IoU) have been measured. IoU is the metric for estimating the amount of overlap between the original mask and the predicted mask where the higher value indicates good prediction and validity in

TABLE II: Performance comparison between small and comparatively large datasets.

No of Images	Model	IoU Scroe (%)	Dice Score (%)
10	U-Net	82.97	90.59
	U-Net++	13.42	23.09
110	**U-Net**	**84.33**	**91.34**
	U-Net++	17.06	28.27

checked through this evaluation metric. On the other hand, Dice coefficient that double counts the intersection and shows how the masks overlap. Equation 12 and 13 shows the equation to calculate IoU and dice coefficient, respectively [1]. Here TP, TN, FP, FN represents True Positive, True Negative, False Positive and False Negative values respectively. These are very useful to understand the overlap between ground truth and predicted area of hemorrhage. Table II shows the best IoU score is 84.33% and dice score is 91.34% which have been achieved on the enriched dataset by U-Net. U-Net++ has gave a lower IoU and dice score on both datasets.

$$IoU = \frac{TP}{TP + FN + FP} \tag{12}$$

$$Dice = \frac{2 \times TP}{2 \times TP + FN + FP} \tag{13}$$

In image segmentation task, the U-net model has given a satisfactory result by achieving 82.97% IoU and 90.59% dice coefficient while using the small dataset. But after enriching the dataset by applying non-linear transformation on the dataset, the IoU score increased about 1.36% and dice score increased almost 1%. While using the U-Net++ architecture, the model architecture is more complex and the amount of data are not enough for such model. The effect of small amount of data on complex architecture can be seen in the IoU and dice score that is much lower than the result of U-Net model. The dataset is still not enough for training and evaluation for any deep learning model which became the obstruction of getting more than the previous accuracy.

B. Qualitative Result of Segmentation

Fig. 4 shows a sample image and its mask. The prediction of the U-net model on 10 test images is shown in Fig. 5(a). From the overlay shown in the right side, it is easily understandable how correctly the model predicts.

Also the result on 110 test images from enriched dataset has been shown in Fig. 5(b), which would help to differentiate how better the predictions are from the small dataset. Fig. 5(c) and 5(d) shows the segmentation results of U-Net++ on small and large datasets, respectively. The model segmented the skull of the brain as hemorrhage. Overlays in all these images show how much the prediction differs from the original mask where the red portion is for predicted masks and the transparent white portion is the actual area of hemorrhage.

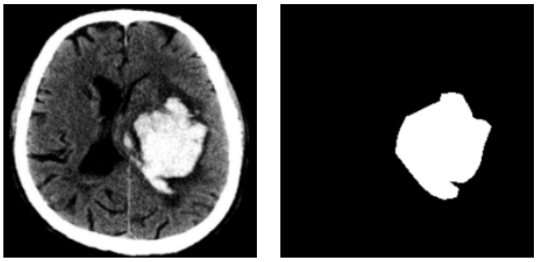

Fig. 4: Sample of original image and mask.

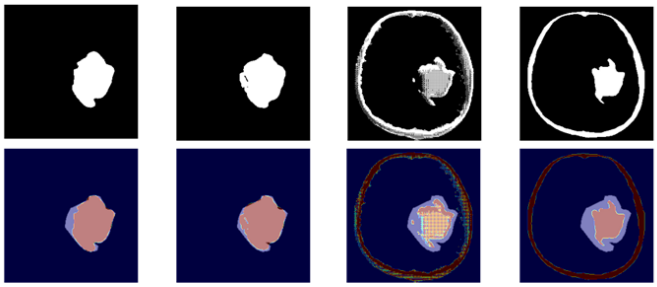

(a) U-Net on small dataset (b) U-Net on large dataset (c) U-Net++ on small dataset (d) U-Net++ on large dataset

Fig. 5: Visualization of image segmentation using U-Net and U-Net++ on small and large dataset.

V. Conclusion

A custom segmentation dataset has been developed by annotating manually using the Head-CT hemorrhage [15] dataset. The hemorrhagic regions have been annotated and performed a segmentation operation using U-Net architecture. After getting good result on a small dataset with 66 images, two non-linear transformations, twirl and spherical transformation have been applied on 66 images and the enriched dataset has got 716 images. The model was successful in producing an excellent outcome. To observe how more complex model works on these datasets, U-Net++ model has also been used but the performance was noticeably inferior to that of U-Net model. The main limitation in this work is the dataset that can be solved by adding variation in this dataset. As for future works, variation in this dataset can be added by following different techniques. After segmenting the hemorrhagic areas, which type of hemorrhage occured can be classified. Some other approaches for hemorrhage segmentation can be observed. Hence different models can be applied on our segmentation dataset.

References

[1] L. Li, M. Wei, B. Liu, K. Atchaneeyasakul, F. Zhou, Z. Pan, S. A. Kumar, J. Y. Zhang, Y. Pu, D. S. Liebeskind *et al.*, "Deep learning for hemorrhagic lesion detection and segmentation on brain ct images," *IEEE journal of biomedical and health informatics*, vol. 25, no. 5, pp. 1646–1659, 2020.

[2] W. F. McCORMICK and D. B. ROSENFIELD, "Massive brain hemorrhage: a review of 144 cases and an examination of their causes," *Stroke*, vol. 4, no. 6, pp. 946–954, 1973.

[3] M. K. Abraham and W.-T. W. Chang, "Subarachnoid hemorrhage," *Emergency Medicine Clinics*, vol. 34, no. 4, pp. 901–916, 2016.

[4] M. F. Sharrock, W. A. Mould, H. Ali, M. Hildreth, I. A. Awad, D. F. Hanley, and J. Muschelli, "3d deep neural network segmentation of intracerebral hemorrhage: development and validation for clinical trials," *Neuroinformatics*, vol. 19, no. 3, pp. 403–415, 2021.

[5] O. Ronneberger, P. Fischer, and T. Brox, "U-net: Convolutional networks for biomedical image segmentation," in *International Conference on Medical image computing and computer-assisted intervention*. Springer, 2015, pp. 234–241.

[6] Z. Zhou, M. M. Rahman Siddiquee, N. Tajbakhsh, and J. Liang, "Unet++: A nested u-net architecture for medical image segmentation," in *Deep learning in medical image analysis and multimodal learning for clinical decision support*. Springer, 2018, pp. 3–11.

[7] V. Davis and S. Devane, "Diagnosis & classification of brain hemorrhage," in *2017 international conference on advances in computing, communication and control (ICAC3)*. IEEE, 2017, pp. 1–6.

[8] A. H. Ali, S. I. Abdulsalam, and I. S. Nema, "Detection and segmentation of hemorrhage stroke using textural analysis on brain ct images," *International Journal of Soft Computing and Engineering (IJSCE), ISSN*, pp. 2231–2307, 2015.

[9] A. Muhammad and W. Guojun, "Segmentation of calcification and brain hemorrhage with midline detection," in *2017 IEEE International Symposium on Parallel and Distributed Processing with Applications and 2017 IEEE International Conference on Ubiquitous Computing and Communications (ISPA/IUCC)*. IEEE, 2017, pp. 1082–1090.

[10] A. Majumdar, L. Brattain, B. Telfer, C. Farris, and J. Scalera, "Detecting intracranial hemorrhage with deep learning," in *2018 40th annual international conference of the IEEE engineering in medicine and biology society (EMBC)*. IEEE, 2018, pp. 583–587.

[11] M. Naidu, P. R. Kumar, and K. Chiranjeevi, "Shannon and fuzzy entropy based evolutionary image thresholding for image segmentation," *Alexandria engineering journal*, vol. 57, no. 3, pp. 1643–1655, 2018.

[12] X. Zheng, Q. Lei, R. Yao, Y. Gong, and Q. Yin, "Image segmentation based on adaptive k-means algorithm," *EURASIP Journal on Image and Video Processing*, vol. 2018, no. 1, pp. 1–10, 2018.

[13] M. R. Islam, M. R. Imteaz *et al.*, "Detection and analysis of brain tumor from mri by integrated thresholding and morphological process with histogram based method," in *2018 international conference on computer, communication, chemical, material and electronic engineering (IC4ME2)*. IEEE, 2018, pp. 1–5.

[14] D. Zhou and Y. Shao, "Region growing for image segmentation using an extended pcnn model," *IET Image Processing*, vol. 12, no. 5, pp. 729–737, 2018.

[15] F. Kitamura, "Head CT - hemorrhage — Kaggle," https://www.kaggle.com/felipekitamura/head-ct-hemorrhage, [Online; accessed 21-March-2022].

[16] A. Dutta and A. Zisserman, "The via annotation software for images, audio and video," in *Proceedings of the 27th ACM international conference on multimedia*, 2019, pp. 2276–2279.

[17] T. B. Moeslund, *Introduction to video and image processing: Building real systems and applications*. Springer Science & Business Media, 2012.

[18] N. Siddique, S. Paheding, C. P. Elkin, and V. Devabhaktuni, "U-net and its variants for medical image segmentation: A review of theory and applications," *Ieee Access*, vol. 9, pp. 82 031–82 057, 2021.